

Optimizing quantum-enhanced Bayesian multiparameter estimation in noisy apparatus

Federico Belliardo,¹ Valeria Cimini,² Emanuele Polino,² Francesco Hoch,² Bruno Piccirillo,^{3,4} Nicolò Spagnolo,² Vittorio Giovannetti,^{1,*} and Fabio Sciarrino^{2,†}

¹*NEST, Scuola Normale Superiore and Istituto Nanoscienze-CNR, I-56126 Pisa, Italy*

²*Dipartimento di Fisica, Sapienza Università di Roma, Piazzale Aldo Moro 5, I-00185 Roma, Italy*

³*Department of Physics “E. Pancini”, Università di Napoli “Federico II”, Complesso Universitario MSA, via Cintia, 80126, Napoli*

⁴*INFN, Sez. di Napoli, Complesso Universitario di Monte Sant’Angelo, via Cinthia, 80126 Napoli, Italy*

Achieving quantum-enhanced performances when measuring unknown quantities requires developing suitable methodologies for practical scenarios, that include noise and the availability of a limited amount of resources. Here, we report on the optimization of quantum-enhanced Bayesian multiparameter estimation in a scenario where a subset of the parameters describes unavoidable noise processes in an experimental photonic sensor. We explore how the optimization of the estimation changes depending on which parameters are either of interest or are treated as nuisance ones. Our results show that optimizing the multiparameter approach in noisy apparatus represents a significant tool to fully exploit the potential of practical sensors operating beyond the standard quantum limit for broad resources range.

The goal of quantum metrology is to estimate a set of physical parameters, exploiting quantum resources to achieve improved performances beyond those achievable by classical methods. The use of quantum probes discloses the capability to reach the Heisenberg limit (HL), gaining a quadratic scaling advantage over the standard quantum limit (SQL) corresponding to the use of N independent probes [1–5]. Often in a real scenario, even if the interest relies on a single parameter, the process is unavoidably affected by the presence of unknown noises. For these reasons, it is usually more effective to treat these estimations using a multiparameter approach [6–10]. Despite their importance, experimental demonstrations of quantum enhanced estimation in the multiparameter case are still few and limited to modest amounts of coherent quantum resources [5, 11–15]. The following two extremal scenarios are prototypical for multiparameter metrology. In the first case, all the unknown parameters are treated on the same level, and thus one needs to optimize the overall amount of information extracted. Here, the adoption of quantum probes can provide improved performances with respect to strategies where each parameter is estimated separately [16–19]. In the second extremal case, only one parameter is considered to be of interest, but the dynamics of the metrological evolution intrinsically involves other nuisance parameters, of which an approximate knowledge is although necessary to retrieve a good estimator for the desired one. For instance, we have to deal with this scenario when different sources of noise affect the evolution: phase and visibility [20–23], phase and phase diffusion [24, 25], magnetic field and decoherence [26] for example. The optimal strategy in this case is very different from the optimal one in the former scenario, since now the interest is to maximize the information extracted on one parameter at the expense of all the others [27]. In the general case, intermediate configurations between these two extremal scenarios can be defined, corresponding to different choices of the cost

function. For example, a couple of parameters could be considered of interest while the others are treated as nuisance. For each specific scenario, different strategies may thus turn out to be optimal. In general, the importance of the different parameters can be weighted arbitrarily.

Another crucial aspect for quantum metrology in a practical scenario regards the availability of a finite amount of resources N in the estimation process. The standard approach is based on a theoretical framework that is dedicated to define bounds and strategies in the asymptotic limit of large N . However, when only a finite amount of resources is available, any estimation strategy needs to be tailored to optimize the convergence for low values of N [28–30]. A powerful tool here is represented by adaptive protocols, which enable faster convergences to the ultimate limits [31, 32]. These have been implemented both through online [33, 34] and offline [35, 36] approaches also resorting to the use of different machine learning algorithms [37–39]. These techniques demonstrated two relevant characteristics, namely fast convergence to the ultimate bounds and performances independent of the particular value of the parameter of interest. Different experimental applications of adaptive techniques have been reported, first in single-parameter estimation problems [38–43] and then in a multiparameter setting [14, 44]. In this scenario, the versatility of the multiparameter approach allows to choose the optimal allocation of resources, depending on which are the parameters of interest and which are the ones associated to noise processes, treated instead as nuisances.

In this work, we investigate a multiparameter estimation scenario, where the parameters of interest are physical rotation angles [45, 46] together with the noise parameters involved in the interferometric measurements. To this end, we employ orbital angular momentum (OAM) of single photons, carrying tunable OAM values up to 50, able to show N0ON-like sensitivities for rotation estimations [47–52]. Importantly, we extend the single parameter study [48] to a multiparameter approach within a Bayesian framework [30, 53–55] for all the aforementioned scenarios by employing an adaptive strategy ensuring the optimal allocation of resources [56]. Such approach allows us to extend the multiparameter estimation

* vittorio.giovannetti@sns.it

† fabio.sciarrino@uniroma1.it

problems to the regime of $O(30,000)$ number of quantum-like resources, experimentally demonstrating sub-SQL precision in the estimation of the rotation angle for wide resources ranges even with nuisance parameters. In order to quantify the quality of the reached performances, we define non-tight Bayesian bounds on the estimations in each considered scenario.

Precision bounds- The goal of multiparameter quantum metrology is to identify regimes where the estimation precision outperforms the one achievable by classical probes. A crucial aspect is to keep such enhanced performances as the employed resources increase. It becomes key to develop a platform able to investigate such regime with quantum scaling of the precision. Here, we study the simultaneous estimation, in the large resource regime, of a rotation angle $\theta \in [0, \pi)$ and of a collection of parameters (the fringe visibilities V_{s_1}, \dots, V_{s_4} defined below) that affect the efficiency of the detection process [47]. More specifically, in our scheme, before each measurement step we preselect a control parameter s out of a set of four possible values $\{s_1 = 1, s_2 = 2, s_3 = 11, s_4 = 51\}$. In the ideal (noiseless) scenario such choice is meant to force the interferometer to produce a single-photon, N00N-like output state analogous to those employed in [41] to achieve quantum limited precision, i.e. the vector $|\psi_s(\theta)\rangle := \frac{1}{\sqrt{2}}(|0\rangle + e^{-2is\theta}|1\rangle)$, with $|0\rangle, |1\rangle$ being orthogonal circular polarization states. Unfortunately, the selection of high values of s also has the indirect effect to add noise into the model which ultimately deteriorates the visibility of the measurements we perform on $|\psi_s(\theta)\rangle$ to recover θ . Our scheme relays on two different types of detections, the first corresponding to the projection of $|\psi_s(\theta)\rangle$ on the basis $\{(|0\rangle \pm |1\rangle)/\sqrt{2}\}$, while the second uses $\{(|0\rangle \pm i|1\rangle)/\sqrt{2}\}$ as reference basis: in both cases the choice of s will decrease the visibility to the same value $V_s \in [0, 1]$, that one could determine from the measured data. Our interest lies in determining how the estimation precision changes depending on the different perspective from which the multiparameter problem is addressed. To this end, we apply the Bayesian algorithm in Ref. [56]. This procedure identifies the most effective adaptive strategy depending on the different roles assigned to each parameter (i.e. $\theta, V_{s_1}, V_{s_2}, V_{s_3}$, and V_{s_4}), whether they are of interest or are treated as nuisance parameters. In this protocol, the Bayesian posterior probability distribution for all the parameters is represented by a particle filter. From the information accumulated in it, at each step, a greedy strategy selects the experimental settings that minimizes the future expected weighted sum of the estimator variances [56]. In our case, we select both the value s that determines the successive probe state and which basis for the polarization measurement we are supposed to use for the measurements of the associated output state $|\psi_s(\theta)\rangle$. These are the controls that the Bayesian procedure for experimental design will optimize. To quantify the efficiency of the estimation, we define a suitable figure of merit and derive bounds limiting its minimal achievable value for the investigated metrological task. For this purpose given $N \gg 1$ integer, we focus on a generic experimental run \mathbf{r}_N composed by series of individual measurements where, given $i \in \{1, \dots, 4\}$, the control value s_i

is used ν_i times, and it is selected under the global constraint $N = \sum_{i=1}^4 \nu_i s_i$ (this is the total number of resources [2] we dedicate to the recovering of the parameters, with our N00N-like states, see [57] for details). More precisely, \mathbf{r}_N is a string containing the list of selected values of s , the polarization basis chosen for each photon and the outcome of each measurement, see the Supplementary Information [57] for more details. Hence, indicating with $\hat{\theta}^{(\mathbf{r}_N)}, \hat{V}_{s_1}^{(\mathbf{r}_N)}, \dots, \hat{V}_{s_4}^{(\mathbf{r}_N)}$ the estimated values of $\theta, V_{s_1}, \dots, V_{s_4}$ we get from the procedure, we gauge the associated error via the quantity $\Delta_{\mathbf{r}_N, G}^2(\theta) := G_{1,1}|\hat{\theta}^{(\mathbf{r}_N)} - \theta|^2 + \sum_{i=1}^4 G_{i+1, i+1}|\hat{V}_{s_i}^{(\mathbf{r}_N)} - V_{s_i}|^2$, where G is a weight matrix that controls which parameters are to be treated as nuisance and which are the parameters of interest [27]. We repeat the whole estimation for a random collection $\theta_1, \theta_2, \dots, \theta_J$ of J different values of θ , and for each θ_j , run the whole procedure M times. We choose J different rotation angles each measured $M > 200$ times. This finally leads us to the identification of the following figure of merit:

$$\mathcal{M}_G^2 := \text{Median}\left[\frac{1}{J} \sum_{j=1}^J \Delta_{\mathbf{r}_N, G}^2(\theta_j)\right], \quad (1)$$

which we express in terms of the median instead of the expectation value on the Bayesian posterior distribution, due to the fact that the former is much less sensitive to outliers that are always present in the task of rotation estimation [48]. It is possible to impose a theoretical lower limit on (1) which can be used to evaluate the quality of our experimental data. Specifically, we can write:

$$\mathcal{M}_G^2 \gtrapprox \xi C_G / N, \quad (2)$$

with C_G being a constant determined by solving numerically an optimization for the Mean Square Error (MSE) of the estimation, and ξ a pre-factor that helps in translating the MSE bound into an inequality for the median error [57].

Experimental apparatus - In order to investigate a multiparameter metrological problem, we employ a state-of-the-art experimental apparatus, that allows to generate single-photon high-OAM value states showing quantum-like sensitivities for the estimation of a rotation angle. Importantly, we extend the result from the single parameter case [48] to a multiparameter one, exploring unprecedented regimes for multiparameter quantum metrology. The experimental setup is composed of a series of q-plates [48, 58] with an increasing topological charge q arranged in a cascade configuration as reported in Fig. 1. Starting from single photons prepared in the horizontal polarization state, we can generate a NOON-like state in the OAM degree of freedom of the form: $\frac{1}{\sqrt{2}}(|0\rangle|m\rangle + |1\rangle| -m\rangle)$, where $|0, 1\rangle$ refers to the circular polarization, while $|\pm m\rangle$ with $m = 2q$ represents the OAM state and depends on the activated q-plate. The prepared state is then sent to a measurement stage composed of the same set of q-plates in reverse order, allowing to reconvert the OAM state into a polarization state. Such measurement stage can be rotated by an angle $\theta \in [0, \pi)$ by means of a fully motorized rotation cage, as realized in Ref. [48]. In this way, the photon state passing through the full setup becomes the vector $|\psi_s(\theta)\rangle$ defined

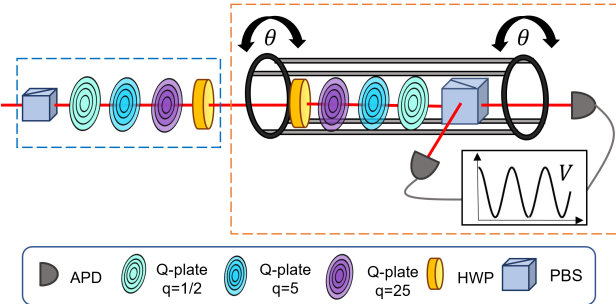


FIG. 1. Sketch of the experimental setup. Single photons are sent through the apparatus consisting of a generation stage (blue rectangle) and a measurement stage (orange rectangle). The first is composed by a polarizing beam splitter (PBS) and three q-plates with different topological charges $q = 1/2; 5; 25$, respectively, followed by a half-waveplate (HWP). The measurement stage is composed by the same elements of the preparation mounted in a compact and motorized cage which can be rotated by an angle θ . After the final PBS, the photons are measured through avalanche photodiodes (APDs). The measurement HWP allows to set the polarization measurement basis.

earlier, where $s = 2q + 1$ is the total angular momentum of the photon. By appropriately choosing the active q-plate, the imparted value of m changes, giving the possibility to tune the frequency of the oscillation interference fringes. Finally, through a half-waveplate after the q-plate, it is possible to select also the measurement polarization basis. Given the employed devices, we have access to states with $s = 1, 2, 11, 51$. The first is obtained when no q-plate is activated, while the others are achieved activating in turn one and only one of the three mounted q-plates in the preparation stage, and the corresponding one in the receiver. These states generate oscillation patterns, retrieved from measurements in polarization basis and characterized by visibilities V_s which depend upon the selected s .

Results and discussion - We start measuring the angle θ while treating the visibilities as nuisance unavoidable noises. To this end, we set the weight matrix G in Eq. (1) to have $G_{11} = 1$ as the only non-null entry. The data analysis is performed offline, and the raw data contains the outcome of the polarization measurement at the end of the receiving apparatus for many photons, for each rotation angle, q-plate, and polarization basis considered. We perform such measurements for $J = 8$ different rotation angles in $[0, \pi]$, which corresponds to the periodicity interval of the system. On such collected measurement results we perform the Bayesian analysis setting the prior distributions on the visibilities as uniform in $[0, 1]$, like the prior on the angle which is uniform in $[0, \pi]$. With the objective of minimizing the median error on the estimation of the rotation angle, the adaptive algorithm selects at each step the most appropriate quantum-like resource among the available ones. This is shown in the inset of Fig. 2a, where the estimation precision on the rotation angle is optimized by increasing gradually the momentum of the generated OAM states. The precision figure of merit achieved with such optimization strategy is reported in the main plot of Fig. 2a), where the ex-

perimental data are compared with the bound on the median in Eq (2), the Standard Quantum Limit (SQL) $1/N$ and the ultimate Heisenberg limit (HL) π^2/N^2 [59]. The confidence interval for the median (plotted in light red) is evaluated with a bootstrap procedure for a 99% confidence level. The experimental results show that the obtained error approaches the computed bound, which proves to be a valid reference even if non-tight. Notably, in such scenario, even if the visibility values are completely unknown, the implemented multiparameter protocol shows an enhanced estimation precision compared to the SQL for a large resources range, previously unexplored by multiparameter estimation experiments. Importantly, differently from [48] where the measurement strategy has been precalibrated according to the visibility values, here we show that it is still possible to obtain a non-negligible region showing sub-SQL performances treating the 4 visibilities as nuisance parameters.

Then, we face the scenario where the visibilities are not treated anymore as nuisances but become themselves parameters which have to be estimated. This happens for instance if the user is interested in the full characterization of an interferometer, therefore needing an estimation of the noise levels. It is interesting to see how the optimization of the available resources changes in these new configurations. In particular, we shall focus on the scenario where one is interested in the estimation of the rotation angle and one of the visibilities (the i_0 -th one), while the remaining ones are still treated as nuisance parameters. Under this assumption, the parameters of interest are the pair $(\theta, V_{s_{i_0}})$ with the median of the associated error computed by taking $G_{1,1} = G_{i_0,i_0} = 1$ in Eq. (1) as the only non-zero elements. As shown in Fig. 2, under this circumstance the Bayesian protocol, although switching to higher dimensional OAM states to decrease the error on the rotation angle, continues to use the q-plate related to the visibility chosen: this is necessary to obtain a good precision on the joint error. The results of the estimation of each of the four possible couples are reported in Fig. 2b, c, d and e. In particular, the plateaus in Fig. 2d and Fig. 2e appear since, for few resources, the q-plates corresponding to $s = 11$ and $s = 51$ are not significantly used. Therefore, the estimator of the corresponding visibilities remains the mean value of the uniform prior distribution in $[0, 1]$, i.e. 0.5, while the error on the phase decreases, thereby reaching a plateau determined by the value of the visibility V_{i_0} itself. This changes only when the algorithm starts to use the high charge q-plates, and the error finally decreases. As a final observation, we notice that in the case where one focuses only on the phase θ there is still a pretty large region in which the slope of the estimation error with sub-SQL performances (specifically looking at Fig. 2a), this happens for values of N between 2000 and 5000). Such behavior on the contrary is depressed when considering the estimation of the pairs $(\theta, V_{s_{i_0}})$ (only for $i_0 = 4$ there is a clear reminiscence of this, see Fig. 2e)). The reason for such behavior is related to the observation that the visibility is an inherently classical parameter and cannot benefit from the high angular momenta representing our quantum resources. We note that, the precision on the rotation angle maintains sub-SQL performances also in all the considered joint estimation

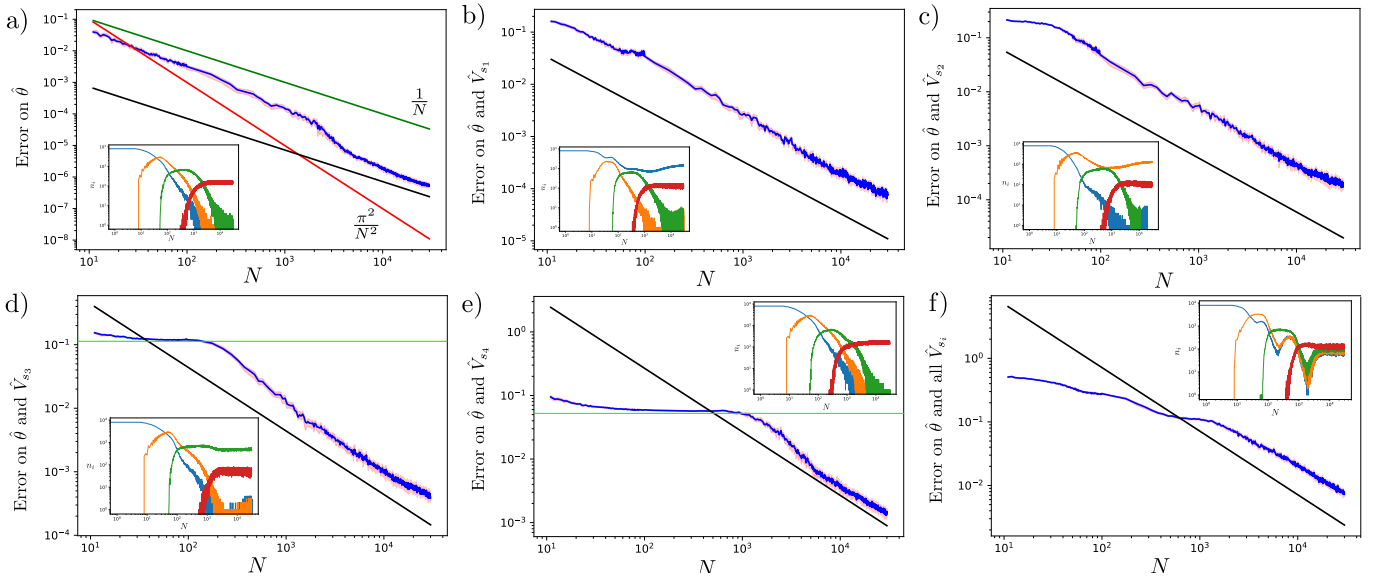


FIG. 2. a) Plot of the median error for the phase only, with all the other parameters treated as nuisance parameters. The green line is the $\text{SQL} = 1/N$, and the red one the $\text{HL} = \pi^2/N^2$. For all the plots the inserts are the number of uses of each q-plate in a batch of 10^3 experiments for each of the $J = 8$ angles as a function of the number of resources. In the inserts the blue lines correspond to photons with no OAM, the orange lines to $s = 2$, the green lines to $s = 11$ and the red ones to $s = 51$. The intersection of these lines corresponds to the point at which the algorithm starts to suggest a q-plate with higher topological charge to perform the next experiment. Plots b), c), d), and e) refer respectively to the joint median error of the phase and each visibility V_{s_1} , V_{s_2} , V_{s_3} and V_{s_4} . For each plot, all the other three visibilities are treated as nuisance parameters. Plot f) represents the precision for the phase and the joint estimation of all the four visibilities. The light green lines in d) and e) highlight the plateaus in the precision, that are discussed in the main text. The d) and e) plots show a scaling (slope of the black line) that in a limited region outperforms the classical ones. In all plots, the black line is the bound in Eq. (2) computed for the appropriate weight matrix G .

scenarios. However, such enhanced performances are visible in the joint estimation errors of (θ, V_4) , see Fig. 2e) where the precision on the visibility parameter does not spoil the overall performances.

In summary, quantum sensing promises to be one of the first quantum technologies exploited to enhance tasks with respect to what is achievable with classical resources. Most of the realistic metrological problems involve more than one unknown parameter, which led to the birth of multiparameter quantum metrology. In this context, a fundamental problem is to optimally allocate the finite available resources, depending on which parameters are treated as nuisance noises and which are the parameters of interest. Furthermore, a crucial step is to reach quantum enhanced multiparameter estimations in a regime of large resources, where experimental demonstrations lack. In this work, we accomplished both these tasks by realizing a photonic setup with quantum elements (the q-plates) and considering different scenarios where the parameter of interest can be either the rotation angle only or the angle and the fringes visibility, treating the others as nuisance in the precision figure of merit. We experimentally showed that this approach is able to reach quantum-like performances in the estimation problems even when unknown nuisance noises are present, for a resources range $O(30,000)$. On one side, the obtained results have shown the possibility of extending the advantages of multiparameter quantum metrology in the large resource domain. On the other, the methodology here described can find application in large varieties of experimen-

tal platforms for quantum sensing, thus representing a tool for future generations of quantum sensors.

ACKNOWLEDGMENTS

The Bayesian data analysis has been programmed with the Python framework PyTorch and ran on a GPU. The code can be found on github [60]. We gratefully acknowledge computational resources of the Center for High Performance Computing (CHPC) at SNS. This work is supported by the ERC Advanced grant PHOSPHOR (Photonics of Spin-Orbit Optical Phenomena; Grant Agreement No. 828978), by the Amaldi Research Center funded by the Ministero dell’Istruzione dell’Università e della Ricerca (Ministry of Education, University and Research) program “Dipartimento di Eccellenza” (CUP:B81I18001170001) and by MIUR (Ministero dell’Istruzione, dell’Università e della Ricerca) via project PRIN 2017 “Taming complexity via QUantum Strategies a Hybrid Integrated Photonic approach” (QUSHIP) Id. 2017SRNBRK.

[1] V. Giovannetti, S. Lloyd, and L. Maccone, *Science* **306**, 1330 (2004).

[2] V. Giovannetti, S. Lloyd, and L. Maccone, *Phys. Rev. Lett.* **96**, 010401 (2006).

[3] V. Giovannetti, S. Lloyd, and L. Maccone, *Nat. Photonics* **5**, 222 (2011).

[4] M. Barbieri, *PRX Quantum* **3**, 010202 (2022).

[5] E. Polino, M. Valeri, N. Spagnolo, and F. Sciarrino, *AVS Quantum Science* **2**, 024703 (2020).

[6] J. Liu, H. Yuan, X.-M. Lu, and X. Wang, *Journal of Physics A: Mathematical and Theoretical* **53**, 023001 (2019).

[7] J. Suzuki, Y. Yang, and M. Hayashi, *Journal of Physics A: Mathematical and Theoretical* **53**, 453001 (2020).

[8] J. Suzuki, *Journal of Physics A: Mathematical and Theoretical* **53**, 264001 (2020).

[9] Magdalena, T. Baumgratz, and A. Datta, *Advances in Physics: X* **1**, 621 (2016), <https://doi.org/10.1080/23746149.2016.1230476>.

[10] F. Albarelli, M. Barbieri, M. G. Genoni, and I. Gianani, *Physics Letters A* **384**, 126311 (2020).

[11] E. Polino, M. Riva, M. Valeri, R. Silvestri, G. Corrielli, A. Crespi, N. Spagnolo, R. Osellame, and F. Sciarrino, *Optica* **6**, 288 (2019).

[12] L.-Z. Liu, Y.-Z. Zhang, Z.-D. Li, R. Zhang, X.-F. Yin, Y.-Y. Fei, L. Li, N.-L. Liu, F. Xu, Y.-A. Chen, *et al.*, *Nature Photonics* **15**, 137 (2021).

[13] S. Hong, Y.-S. Kim, Y.-W. Cho, S.-W. Lee, H. Jung, S. Moon, S.-W. Han, H.-T. Lim, *et al.*, *Nature communications* **12**, 1 (2021).

[14] M. Valeri, V. Cimini, S. Piacentini, F. Ceccarelli, E. Polino, F. Hoch, G. Bizzarri, G. Corrielli, N. Spagnolo, R. Osellame, *et al.*, *arXiv preprint arXiv:2208.14473* (2022).

[15] V. Cimini, M. Valeri, E. Polino, S. Piacentini, F. Ceccarelli, G. Corrielli, N. Spagnolo, R. Osellame, and F. Sciarrino, *arXiv preprint arXiv:2209.00671* (2022).

[16] P. C. Humphreys, M. Barbieri, A. Datta, and I. A. Walmsley, *Physical Review Letters* **111**, 070403 (2013).

[17] W. Górecki and R. Demkowicz-Dobrzański, *Phys. Rev. Lett.* **128**, 040504 (2022).

[18] F. Belliardo and V. Giovannetti, *New Journal of Physics* **23**, 063055 (2021).

[19] J.-D. Yue, Y.-R. Zhang, and H. Fan, *Scientific Reports* **4** (2014), 10.1038/srep05933.

[20] E. Roccia, V. Cimini, M. Sbroscia, I. Gianani, L. Ruggiero, L. Mancino, M. G. Genoni, M. A. Ricci, and M. Barbieri, *Optica* **5**, 1171 (2018).

[21] E. Roccia, I. Gianani, L. Mancino, M. Sbroscia, F. Somma, M. G. Genoni, and M. Barbieri, *Quantum Science and Technology* **3**, 01LT01 (2017).

[22] V. Cimini, I. Gianani, L. Ruggiero, T. Gasperi, M. Sbroscia, E. Roccia, D. Tofani, F. Bruni, M. A. Ricci, and M. Barbieri, *Physical Review A* **99**, 053817 (2019).

[23] V. Cimini, M. Mellini, G. Rampioni, M. Sbroscia, L. Leoni, M. Barbieri, and I. Gianani, *Optics Express* **27**, 35245 (2019).

[24] M. D. Vidrighin, G. Donati, M. G. Genoni, X.-M. Jin, W. S. Kolthammer, M. Kim, A. Datta, M. Barbieri, and I. A. Walmsley, *Nature Communications* **5** (2014), 10.1038/ncomms4532.

[25] M. G. Genoni, S. Olivares, and M. G. A. Paris, *Phys. Rev. Lett.* **106**, 153603 (2011).

[26] Y. Matsuzaki, S. C. Benjamin, and J. Fitzsimons, *Phys. Rev. A* **84**, 012103 (2011).

[27] A. Z. Goldberg, I. Gianani, M. Barbieri, F. Sciarrino, A. M. Steinberg, and N. Spagnolo, *Physical Review A* **102**, 022230 (2020).

[28] J. Rubio, P. A. Knott, T. J. Proctor, and J. A. Dunningham, *Journal of Physics A: Mathematical and Theoretical* **53**, 344001 (2020).

[29] J. Rubio and J. Dunningham, *New Journal of Physics* **21**, 043037 (2019).

[30] J. Rubio and J. Dunningham, *Physical Review A* **101**, 032114 (2020).

[31] H. M. Wiseman, *Physical Review Letters* **75**, 4587 (1995).

[32] D. W. Berry and H. M. Wiseman, *Physical review letters* **85**, 5098 (2000).

[33] A. A. Berni, T. Gehring, B. M. Nielsen, V. Händchen, M. G. Paris, and U. L. Andersen, *Nature Photonics* **9**, 577 (2015).

[34] V. Cimini, M. Mellini, G. Rampioni, M. Sbroscia, L. Leoni, M. Barbieri, and I. Gianani, *Opt. Express* **27**, 35245 (2019).

[35] A. Hentschel and B. C. Sanders, *Physical Review Letters* **107**, 233601 (2011).

[36] N. B. Lovett, C. Crosnier, M. Perarnau-Llobet, and B. C. Sanders, *Physical Review Letters* **110**, 220501 (2013).

[37] A. Hentschel and B. C. Sanders, *Physical Review Letters* **104**, 063603 (2009).

[38] A. Lumino, E. Polino, A. S. Rab, G. Milani, N. Spagnolo, N. Wiebe, and F. Sciarrino, *Physical Review Applied* **10**, 044033 (2018).

[39] K. Rambhatla, S. E. D'Aurelio, M. Valeri, E. Polino, N. Spagnolo, and F. Sciarrino, *Physical Review Research* **2**, 033078 (2020).

[40] M. A. Armen, J. K. Au, J. K. Stockton, A. C. Doherty, and H. Mabuchi, *Physical Review Letters* **89**, 133602 (2002).

[41] B. L. Higgins, D. W. Berry, S. D. Bartlett, H. M. Wiseman, and G. J. Pryde, *Nature* **450**, 393 (2007).

[42] S. Daryanoosh, S. Slussarenko, D. W. Berry, H. M. Wiseman, and G. J. Pryde, *Nature Communications* **9**, 4606 (2018).

[43] T. Wheatley, D. Berry, H. Yonezawa, D. Nakane, H. Arao, D. Pope, T. Ralph, H. Wiseman, A. Furusawa, and E. Huntington, *Physical Review Letters* **104**, 093601 (2010).

[44] M. Valeri, E. Polino, D. Poderini, I. Gianani, G. Corrielli, A. Crespi, R. Osellame, N. Spagnolo, and F. Sciarrino, *npj Quantum Information* **6**, 92 (2020).

[45] A. Z. Goldberg and D. F. James, *Physical Review A* **98**, 032113 (2018).

[46] A. Z. Goldberg, A. B. Klimov, G. Leuchs, and L. L. Sánchez-Soto, *Journal of Physics: Photonics* **3**, 022008 (2021).

[47] V. D'Ambrosio, N. Spagnolo, L. Del Re, S. Slussarenko, Y. Li, L. C. Kwek, L. Marrucci, S. P. Walborn, L. Aolita, and F. Sciarrino, *Nat. Comm.* **4**, 2432 (2013).

[48] V. Cimini, E. Polino, F. Belliardo, F. Hoch, B. Piccirillo, N. Spagnolo, V. Giovannetti, and F. Sciarrino, *arXiv preprint arXiv:2110.02908* (2021).

[49] R. Fickler, G. Campbell, B. Buchler, P. K. Lam, and A. Zeilinger, *Proceedings of the National Academy of Sciences* **113**, 13642 (2016).

[50] S. M. Barnett and R. Zambrini, *Journal of Modern Optics* **53**, 613 (2006).

[51] A. K. Jha, G. S. Agarwal, and R. W. Boyd, *Physical Review A* **83**, 053829 (2011).

[52] M. Hiekkämäki, F. Bouchard, and R. Fickler, *Phys. Rev. Lett.* **127**, 263601 (2021).

[53] C. W. Helstrom and C. W. Helstrom, *Quantum detection and*

estimation theory, Vol. 84 (Academic press New York, 1976).

- [54] G. E. Box and G. C. Tiao, *Bayesian inference in statistical analysis*, Vol. 40 (John Wiley & Sons, 2011).
- [55] S. E. D'Aurelio, M. Valeri, E. Polino, V. Cimini, I. Gianani, M. Barbieri, G. Corrielli, A. Crespi, R. Osellame, F. Sciarrino, *et al.*, *Quantum Science and Technology* (2022).
- [56] C. E. Granade, C. Ferrie, N. Wiebe, and D. G. Cory, *New Journal of Physics* **14**, 103013 (2012).
- [57] The Supplemental Material accompanying the paper, available from XXXX,.
- [58] L. Marrucci, C. Manzo, and D. Paparo, *Phys. Rev. Lett.* **96**, 163905 (2006).
- [59] W. Górecki, R. Demkowicz-Dobrzański, H. M. Wiseman, and D. W. Berry, *Phys. Rev. Lett.* **124**, 030501 (2020).
- [60] F. Belliardo, “Bayesian multiparameter,” https://github.com/fedebell/AppuntiDottorato/tree/main/bayesian_multiparameter (2022).

Supplementary information for Optimizing quantum-enhanced Bayesian multiparameter estimation in noisy apparatus

Federico Belliardo,¹ Valeria Cimini,² Emanuele Polino,² Francesco Hoch,² Bruno Piccirillo,³ Nicòlo Spagnolo,² Vittorio Giovannetti,^{1,*} and Fabio Sciarrino^{2,†}

¹*NEST, Scuola Normale Superiore and Istituto Nanoscienze-CNR, I-56126 Pisa, Italy*

²*Dipartimento di Fisica, Sapienza Università di Roma, Piazzale Aldo Moro 5, I-00185 Roma, Italy*

³*Department of Physics “E. Pancini”, Università di Napoli “Federico II”, Complesso Universitario MSA, via Cintia, 80126, Napoli*

Supplementary Note 1. Derivation of multiparameter precision bounds

In this section, we derive the multiparameter precision bound of Eq. (2) in the main text. In order to do so, we start from the quantity that we simulate, that are the measurements outcomes. The greedy algorithm selects for each photon consumed in the experiment the best value of s among the available ones and the polarization basis b that give us the maximum information gain. We called \mathbf{r}_N the list of tuples containing these choices, together with the outcomes o i.e.

$$\mathbf{r}_N = \{(s_1, b_1, o_1), (s_2, b_2, o_2), \dots, (s_K, b_K, o_K)\}, \quad (1)$$

Notice that the number of total resources used N and the number of measurements K , i.e. the number of photons are different. The most widely employed figure of merit for the precision of an estimator is the Mean Squared Error (MSE). Given the estimators $\hat{\theta}^{(\mathbf{r}_N)}$ and $\hat{V}_{s_i}^{(\mathbf{r}_N)}$ for θ and V_{s_i} respectively, and a weight matrix G that codifies which parameters are of interests, we have introduced in the main text the error quantity

$$\Delta_{\mathbf{r}_N, G}^2(\theta) := G_{1,1} |\hat{\theta}^{(\mathbf{r}_N)} - \theta|^2 + \sum_{i=1}^4 G_{i+1, i+1} |\hat{V}_{s_i}^{(\mathbf{r}_N)} - V_{s_i}|^2, \quad (2)$$

its expectation value on the experimental run is $\Delta_G^2(\theta) := \mathbb{E}_{\mathbf{r}_N} [\Delta_{\mathbf{r}_N, G}^2(\theta)]$. We then take the expectation value of this precision on the prior distribution for θ and define $\Delta_G^2 := \mathbb{E}_\theta [\Delta_G^2(\theta)]$. We can approximate these expressions by means of M simulations for a discrete and finite number of angles J . So that we can write

$$\Delta_G^2 \simeq \frac{1}{MJ} \sum_{m=1}^M \sum_{j=1}^J \Delta_{\mathbf{r}_N^{m,j}, G}^2(\theta_j), \quad (3)$$

where $\mathbf{r}_N^{m,j}$ is the string characterizing the m -th experimental run for the j -th angle. The figure of merit in Eq. (1) of the main text is computed by taking the median of the M quantities $\sum_{j=1}^J \Delta_{\mathbf{r}_N^{m,j}, G}^2(\theta_j)$ instead of the mean. We now see how the Cramèr-Rao (CR) bound sets a limit to Δ_G^2 and how this can become a bound for the median error \mathcal{M}_G^2 . Depending on the measurement basis chosen, the results $o_1, o_2 \in \{-1, +1\}$ of the two polarization measurements for the i -th q-plate are distributed respectively according to

$$p_1(o_1|\theta, V_{s_i}) := \frac{1}{2} (1 + o_1 \cdot V_{s_i} \cos 2s_i \theta) \quad \text{or} \quad p_2(o_2|\theta, V_{s_i}) := \frac{1}{2} (1 + o_2 \cdot V_{s_i} \sin 2s_i \theta). \quad (4)$$

We have ν_i measurements for the q-plate s_i in total, that we assume being evenly split between the two polarization basis. This is not true in the experiment, since the basis is chosen adaptively, however it is an assumption necessary to proceed in the analytical computation of the bound. From these probabilities we can write the 5×5 Fisher information

* vittorio.giovannetti@sns.it

† fabio.scarrino@uniroma1.it

matrix I (FI matrix) for the five parameters $(\theta, V_{s_1}, V_{s_2}, V_{s_3}, V_{s_4})$, whose non-zero elements are

$$\begin{aligned} I_{11} &= \sum_{i=1}^4 \frac{4s_i^2 V_{s_i}^2 \nu_i (-4 + 3V_{s_i}^2 + V_{s_i}^2 \cos 4s_i \theta)}{-8 + 8V_{s_i}^2 - V_{s_i}^4 + V_{s_i}^4 \cos 4s_i \theta} , \\ I_{i+1,1} &= -\frac{4s_i V_{s_i}^3 \nu_i \cot 2s_i \theta}{(V_{s_i}^2 - \csc^2 s_i \theta)(V_{s_i}^2 - \sec^2 s_i \theta)} , \\ I_{i+1,i+1} &= 2\nu_i \left(\frac{1}{-V_{s_i}^2 + \csc^2 s_i \theta} + \frac{1}{-V_{s_i}^2 + \sec^2 s_i \theta} \right) , \end{aligned}$$

for $i = 1, 2, 3, 4$, and $I_{i+1,1} = I_{1,i+1}$ for symmetry. The Cramér-Rao bound, holding true for asymptotically unbiased estimators, is then expressed by the following inequality involving $\Delta_G^2(\theta)$:

$$\Delta_G^2(\theta) \geq \text{Tr}(G \cdot I^{-1}) , \quad (5)$$

by taking the expectation value on the prior on θ we have

$$\Delta_G^2 = \mathbb{E}_\theta[\Delta_G^2(\theta)] \geq \mathbb{E}_\theta[\text{Tr}(G \cdot I^{-1})] \geq \text{Tr}(G \cdot \mathbb{E}_\theta[I]^{-1}) . \quad (6)$$

We now want to renormalize the uses of each q-plate ν_i in such a way to highlight the dependence on the total number of resources N , i.e. $\nu_i = x_i N$. The FI matrix I becomes $I = N \tilde{I}$, where the entries of \tilde{I} are similar to that of I , only that ν_i is substituted with x_i . The CR bound reads now

$$\Delta_G^2 \geq \frac{\text{Tr}(G \cdot \mathbb{E}_\theta[\tilde{I}]^{-1})}{N} \geq \frac{C_G}{N} , \quad (7)$$

where the expectation value of the matrix \tilde{I} is diagonal with entries

$$\mathbb{E}_\theta[\tilde{I}_{11}] = 4 \sum_{i=1}^4 x_i s_i^2 \left(1 - \sqrt{1 - V_{s_i}^2} \right) , \quad (8)$$

$$\mathbb{E}_\theta[\tilde{I}_{i+1,i+1}] = \frac{4x_i (1 - \sqrt{1 - V_{s_i}^2})}{V_{s_i}^2 \sqrt{1 - V_{s_i}^2}} , \quad \text{for } i = 1, \dots, 4 , \quad (9)$$

and C_G is the solution of the following minimization problem:

$$\begin{cases} C_G = \min_{x_i} \text{Tr}(G \cdot \mathbb{E}_\theta[\tilde{I}]^{-1}) \\ \text{subject to } \sum_{i=1}^4 s_i x_i = 1 \\ x_i \geq 0 \end{cases} . \quad (10)$$

In order to get a reference value for the median error, we suppose that the estimators $\hat{\theta}^{(\mathbf{r}_N)}$ and $\hat{V}_{s_i}^{(\mathbf{r}_N)}$ are asymptotically normal and unbiased. Because the square of the deviations $|\hat{\theta}^{(\mathbf{r}_N)} - \theta_j|^2$ and $|\hat{V}_{s_i}^{(\mathbf{r}_N)} - V_{s_i}|^2$ are left-skewed and independent variables, we observe that

$$\text{Median} \left[\sum_{j=1}^J \Delta_{\mathbf{r}_N, G}^2(\theta_j) \right] \geq \sum_{j=1}^J \text{Median}[|\hat{\theta}^{(\mathbf{r}_N)} - \theta_j|^2] + \text{Median}[|\hat{V}_{s_i}^{(\mathbf{r}_N)} - V_{s_i}|^2] .$$

Under the said hypothesis, the variable $\hat{\theta}^{(\mathbf{r}_N)} - \theta_j$ is a Gaussian centered in zero and the median of its square is proportional to the variance

$$\text{Median} \left[|\hat{\theta}^{(\mathbf{r}_N)} - \theta|^2 \right] = \xi \mathbb{E}_{\mathbf{r}_N} [|\hat{\theta}^{(\mathbf{r}_N)} - \theta|^2] , \quad (11)$$

with a factor $\xi \simeq 0.4549$ that can be estimated numerically. Therefore, the bound on the median error of the estimation is

$$\mathcal{M}_G^2 \gtrapprox \frac{\xi C_G}{N} . \quad (12)$$

Supplementary Note 2. The Bayesian algorithm

In this section, we present the Bayesian algorithm proposed in [1], with the application to our q-plates setup in mind. With respect to the original formulation, we made a few corrections necessary because of the circular nature of the angular variable that we are going to measure. In every experiment, $n_p = 5000$ particles have been used. The parameters to estimate are collected in the vector $\mathbf{x} := (\theta, V_{s_1}, V_{s_2}, V_{s_3}, V_{s_4})$, that contains the phase in the first entry and the four visibilities in the other ones. Being the Granade's method based on a particle filter, it represents internally the posterior probability distribution with the ensemble $\mathcal{E} := \{\mathbf{x}^k, w^k\}$, where \mathbf{x}^k is the position of the k -th particle and w^k its weight. The j -th component of the k -th particle of the ensemble will be represented as x_j^k , and could correspond to the phase if $j = 0$, that is $x_0^k = \theta^k$ or to one of the visibilities if $j = 1, 2, 3, 4$, that is $x_j^k = V_{s_j}^k$. The mean of the angular values is computed as

$$\hat{\mu}_0 := \arg \left[\sum_{i=1}^{n_p} w^k \exp(i\theta^k) \right] , \quad (13)$$

while the mean values of the visibilities are

$$\hat{\mu}_j = \sum_{k=1}^{n_p} w^k V_{s_j}^k . \quad (14)$$

Together they form the vectorial mean of the distribution $\hat{\mu} = (\hat{\mu}_0, \hat{\mu}_1, \hat{\mu}_2, \hat{\mu}_3, \hat{\mu}_4)$. The covariance matrix is defined as

$$\text{Cov}_{ij} := \sum_{k=1}^{n_p} w^k (x_i^k - \hat{\mu}_i)(x_j^k - \hat{\mu}_j) . \quad (15)$$

If $i = 1$ or $j = 1$ then difference in $x_i^k - \hat{\mu}_i$ or $x_j^k - \hat{\mu}_j$ is actually the circular distance

$$d(x_i^k, \hat{\mu}_i) = \pi - |(x_i^k - \hat{\mu}_i) \bmod 2\pi - \pi| . \quad (16)$$

The Bayesian algorithm tries for each new experiment (each new photon sent with a specific q-plate activated) to minimize the scalar variance of the posterior distribution, that is

$$\sigma^2 := \text{Tr} [G \cdot \text{Cov}] = \sum_{i,j} G_{ij} \text{Cov}_{ij} , \quad (17)$$

by simulating each one of the possible 8 experiments (4 q-plates and 2 polarization basis among which we have to choose) and choosing the one with the lowest expected variance. In this way the algorithm attempts to concentrate as much as possible the distribution around its mean, without however planning for more than one step in the future. The simplest possible non-greedy extension of this would be to simulate two measurement steps, this would mean computing 64 possible expected variances. Simulating many more steps becomes quickly unfeasible. The resampling strategy of the Granade procedure in [1] has also undergone minor changes to adapt it to the phase estimation problem.

Details on the data analysis

At difference with the offline algorithm when we run a simulation with a fixed number of photons we cannot exactly fix the total number N of resources, because the stochastic nature of the measurement outcomes propagates to the choice of the next q-plate and therefore to N . However, we can repeat $M \gg 1$ times the simulation, collecting the precision after each used photon in the tuple $(\Delta_{r_n, G}^2(\theta_j), n)$, where n is the total resource number used up to that point. We will then look at all the point with total resources falling in the interval $[n, n + \Delta n]$ with Δn small, and the median error of this cluster is the error we associate to n . We call this operation clustering of the data, and we chose to cluster only the point having $n > 100$. The chosen interval was $\Delta n = 50$.

Supplementary Note 3. Values of the angles and the visibilities

The value of the rotation angle is known from the mechanical platform on which the receiving end of the apparatus is mounted and the visibilities are computed from the non-Bayesian estimator

$$\hat{V} = \sqrt{\frac{\nu \left[(2f_0 - 1)^2 + (2f_+ - 1)^2 \right] - 1}{\nu - 1}}, \quad (18)$$

where f_0 and f_+ are the frequencies of the outcomes $o = 0$ and $o = +$ for the two polarization measurements for a fixed phase and q-plate, and ν is the number of experiments executed for each polarization. These estimators for the visibilities are evaluated prior and independently of the Bayesian procedure. The results will be considered the “true” values of the visibilities in evaluating the precision of the Bayesian approach. These are

θ	V_1	V_2	V_3	V_4
0.00235	0.8776	0.9091	0.8445	0.7038
0.06145	0.9085	0.8934	0.8007	0.7611
0.38000	0.9399	0.9153	0.7936	0.7222
0.49620	0.9211	0.9315	0.7261	0.8186
1.6645	0.9331	0.8914	0.8691	0.7312
1.8750	0.9599	0.9081	0.8762	0.6618
2.5900	0.9187	0.9587	0.8775	0.6848
2.9600	0.8986	0.9321	0.8700	0.7528
-	0.9197	0.9174	0.8322	0.7295

The above table contains the values of the eight angles analyzed in the experiment and their corresponding visibilities for each q-plate configuration. The last line reports the mean values of the visibilities.

Supplementary References

[1] C. E. Granade, C. Ferrie, N. Wiebe, and D. G. Cory, New Journal of Physics **14**, 103013 (2012)